applied sciences

MDPI

Article

Experimental Study on the Difference Mechanism of Shaft Resistance between Uplift Piles and Compressive Piles

Hailong Ma [1,*], Yufei Ma [2], Lin Zhu [1] and Hangyu Zhang [1]

[1] School of Civil Engineering and Architecture, Zhejiang Sci-Tech University, Hangzhou 310018, China
[2] Zhejiang Geological Big Data Application Center Co., Ltd., Hangzhou 310058, China
* Correspondence: mahailonglg@126.com

Abstract: To study the formation mechanism of the lower shaft resistance of uplift piles compared to compression piles, the additional stress caused by uplift and compressive piles in the soil is obtained through indoor model tests with embedded micro earth pressure cells. The study shows that the uplift pile has an unloading effect in pile side soil, and the compressive pile has a loading effect in pile side soil. Closer to the loading point, the unloading effect of the uplift pile and the loading effect of the compressive pile becomes more obvious. The unloading effect decreases the shaft resistance of the uplift pile, and the loading effect increases the shaft resistance of the compressive pile. The tests also reveal that the distribution range of additional stress caused by a single pile is within 6 d from the axis of the pile. After considering the effects of loading and unloading of a single pile, the calculated uplift pile bearing capacity is close to the values of formulas such as Meyerhof and Deshmukh and the measured value.

Keywords: uplift piles; compressive piles; additional stress; shaft resistance; unloading effect; loading effect

check for updates

Citation: Ma, H.; Ma, Y.; Zhu, L.; Zhang, H. Experimental Study on the Difference Mechanism of Shaft Resistance between Uplift Piles and Compressive Piles. *Appl. Sci.* **2023**, *13*, 3158. https://doi.org/10.3390/app13053158

Academic Editor: Raffaele Zinno

Received: 7 February 2023
Revised: 27 February 2023
Accepted: 27 February 2023
Published: 1 March 2023

1. Introduction

Uplift piles are widely used in the anti-floating of underground engineering, anti-uplift of tower foundations of power transmission and transformation engineering, anti-uplift of tower foundation for communication, anti-uplift of high-rise chimney foundation, anti-wind and a wave of offshore platform and other projects. Due to its extensive engineering application, it has aroused interest in research [1–5]. Emirler et al. [6] concluded from model tests that the loading capacity of the uplift pile increases with increasing pile embedment ratio and increasing sand compactness. For dense sandy soils, the load-displacement curve of the uplift resistant pile is a straight line segment before the peak load. Ashour et al. [7] proposed the construction method of the load-displacement curve of uplift piles according to the load transfer curve between the pile-soil interface, where the development of shear stress at the pile-soil interface affects the shape of the load-transfer curve, and also considers the effect of Poisson's ratio and stress relaxation of the pile on the pile bearing capacity. Das et al. [8] found that before the critical embedment ratio of the pile, the unit shaft resistance increased linearly with the pile length, and the critical embedment ratio of the pile was related to the relative density of the soil. Based on the laboratory test, the estimation formula of the ultimate uplift bearing capacity was proposed. According to Meyerhof [9], the uplift shaft resistance of piles under axial load can be expressed by the uplift coefficient. In sandy soil or clay, the greater the inclination of anchor piles, the greater the uplift coefficient of piles. With the increase of the embedment depth of piles, the influence of the inclination of piles on the uplift bearing capacity is weakened. For uplift piles with a given burial depth, when the inclination of piles is less than 45°, the change of the shaft resistance with the pile inclination is not obvious. Chattopadhyay et al. [10] proposed a method for calculating the loading capacity of uplift resistant piles in sandy soils. The influence of the length of the pile, the diameter of the pile, the surface characteristics of the pile, and the soil properties on the bearing capacity can also be considered, and the critical embedment depth of the pile is not only related to the density of the soil, but also to the soil properties. Deshmukh et al. [11] established a formula for calculating the bearing capacity of the uplift pile anchor based on Kötter's formula, which can directly calculate the bearing capacity of the uplift pile without reference to a specific chart, and compared with 28 cases, the predicted results of this method are in good agreement with the case results. According to different failure surfaces of the soil around piles, Meyerhof [9], Chattopadhyay et al. [10], and Deshmukh et al. [11] proposed formulas to calculate the net bearing capacity of uplift piles with similar principles.

It is well known that uplift piles have lower bearing capacity than compressive piles, but there are different understandings of its causes. Tovar-Valencia et al. [12] used digital image correlation (DIC) techniques to model piles with different roughness of the pile surface in sandy soils to obtain displacement and strain fields in sandy soils. The data from DIC showed that the magnitude of the pile surface roughness was related to the shaft resistance and the displacement and strain fields in the soil on the pile side. The greater the pile surface roughness, the greater the pile shaft resistance, and the greater the displacement and strain in the soil. Galvis-Castro et al. [13] considered that the method of using the shaft resistance correction coefficient of the compression pile to obtain the shaft resistance of the uplift pile is limited. They used DIC to perform a compressive static load test on the pile followed by a tensile static load test on the pile, and a tensile static load test on the other pile followed by a compressive static load test on the pile. The ratio of the shaft resistance of the uplift pile to the shaft resistance of the compressive pile is less than 1. The ratio is influenced by the sequence of load application and the roughness of the pile surface, the reason why the shaft resistance of the uplift pile is less than the shaft resistance of the compressive pile is due to the rotation of the principal strain when the load direction is reversed. DeNicola et al. [14] believed that the difference in shaft resistance between uplift piles and compressive piles was caused by the following reasons. First, the diameter of the uplift pile decreases under tensile action, which affects the closeness of the contact between the pile surface and soil. The shaft resistance of the uplift pile decreases, while that of the compressive pile is the opposite, which is caused by the Poisson effect. Second, the stress field in the soil changes: the stress in the soil caused by the uplift pile decreases, while that of the compressive pile increases. Third, the principal stress of the pile side rotates due to different stress directions and causes a change in shaft resistance. Wang et al. [15], Zhang et al. [16], Su et al. [17], and Ou et al. [18] believe that the Poisson effect of piles leads to a lower tensile bearing capacity of piles than the compressive bearing capacity. Wang et al. [19] show that in sandy conditions, when the Poisson's ratio of piles changes from 0.1 to 0.3, the uplift coefficient (bearing capacity of uplift piles/bearing capacity of compressive piles or average shaft resistance of uplift piles/average shaft resistance of compressive piles) changes from 0.993 to 0.980. Therefore, the influence of the Poisson effect on the uplift coefficient is not obvious.

Wang et al. [15], Zhang et al. [16], Su et al. [17], and Ou et al. [18] believe that the Poisson effect of pile leads to a smaller bearing capacity of the tensile pile than that of compression pile, which were not confirmed by calculation. As the Poisson effect does not have a significant effect on the uplift resistance coefficient [19], the low bearing capacity of uplift piles may be caused by the change of additional stress in the soil around the pile [14]. For the additional stress in the soil around the pile, Ma et al. [20,21] used model tests to investigate the distribution of additional stress in soil under different load modes, as well as the effect of additional stress in soil on the interaction between the upper and lower sections of self-anchored test piles. Zhou et al. [22] studied the relationship between stability and horizontal displacement of pile-anchored support structures considering additional stress. In this paper, based on the indoor model tests, the micro earth pressure cells were buried in the pile side soil to quantitatively study the additional stress difference caused by the unloading effect of the uplift pile and the loading effect of the compression pile in the pile side soil, and analyzes the main reasons why the bearing capacity of the uplift pile is less than that of the compression pile.

2. Unloading Effect of Uplift Piles and Loading Effect of Compressive Piles

When upward tension is applied at the top of the uplift pile, a downward shaft resistance (called negative shaft resistance) is generated at the pile side, while upward additional stress σ_z is generated in the soil [23], as shown in Figure 1a. Apply downward pressure at the top of the compression pile, and at this time, the upward shaft resistance (called positive shaft resistance) will be generated at the pile side, while downward additional stress σ_z is generated in the soil [23], as shown in Figure 1b. The upward additional stress has an unloading effect on the pile side soil, while the downward additional stress has a loading effect on the pile side soil. As the shaft resistance is related to the vertical stress in the soil on the side of the pile, the unloading and loading effect of the pile on the soil causes a change in the shaft resistance.

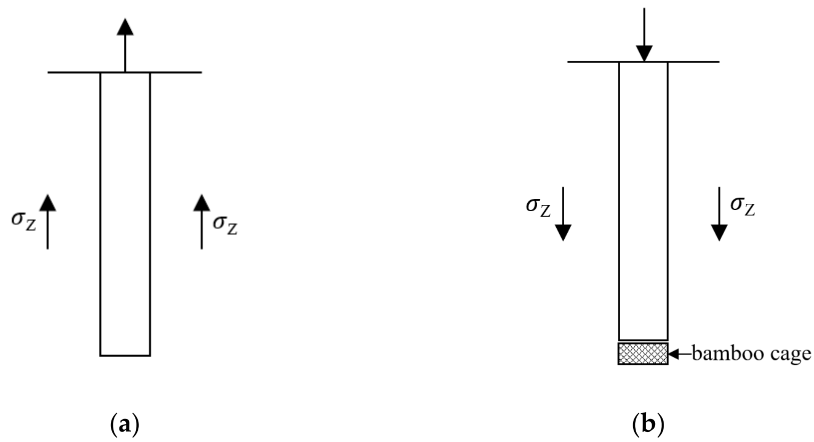

Figure 1. Additional stress caused by uplift piles and compressive piles in soil: (**a**) Uplift pile; (**b**) Compressive pile.

3. Model Test

The test model box is made of welded steel plates, the length, width, and depth of the model box are 1500 mm, 500 mm, and 1700 mm respectively. The soil is made of silt, and the particle size composition of silt is obtained by the particle analysis test, which is shown in Table 1. The model pile is made of plexiglass pipes. The diameter of the model pile is 50 mm, the wall thickness is 8 mm, the lengths of the uplift pile and compressive pile are 1200 mm, and the elastic modulus of the model pile is 2.1 GPa. The soil is made by layered filling in box, and each layer is approximately 200 mm thick. The next layer was filled after 2 days rest period with uniform water sprinkling on top. Using burying methods to set up model piles, the model piles are fixed in the design position in advance and simultaneously buried in the soil when each silt layer is filled. The compressive pile is soil-free at the bottom of the pile. Under the pile, bottom is a hollow bamboo cage with a length of 60 mm and a diameter of 50 mm. During the test, the compressive pile can penetrate the bamboo cage to ensure that the pile bottom does not produce a tip resistance of the pile.

Table 1. Particle size composition of silt.

Particle Diameter (mm)	$d_s < 0.075$	$0.075 \le d_s < 0.15$	$0.15 \le d_s < 0.3$	$d_s \ge 0.3$
Proportion	76.3%	12.3%	7.5%	3.9%

Notation: d_s is particle size.

The additional stress in the soil at the side of the pile is measured using micro earth pressure cells, which are buried according to the design requirements during soil production. In the vertical direction, the micro earth pressure cells are set down at 300 mm below ground level and at 300 mm intervals downwards, i.e., 300 mm, 600 mm, 900 mm, and 1200 mm downwards from ground level. In the horizontal direction, earth pressure cells are buried 75 mm (1.5 d, where d is the pile diameter), 150 mm (3.0 d), 225 mm (4.5 d), and 300 mm (6.0 d) away from the axis of the pile. The layout of earth pressure cells is shown in Figure 2, and the embedment of micro earth pressure cells is shown in Figure 3.

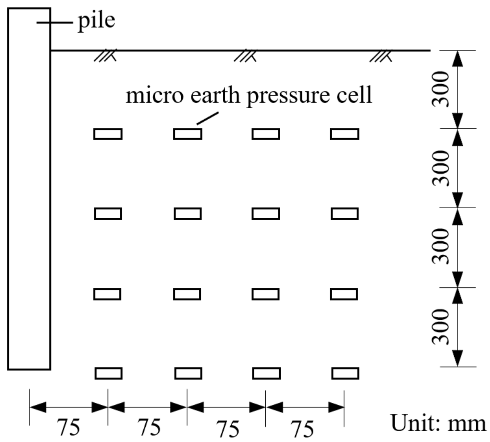

Figure 2. Layout of the earth pressure cells.

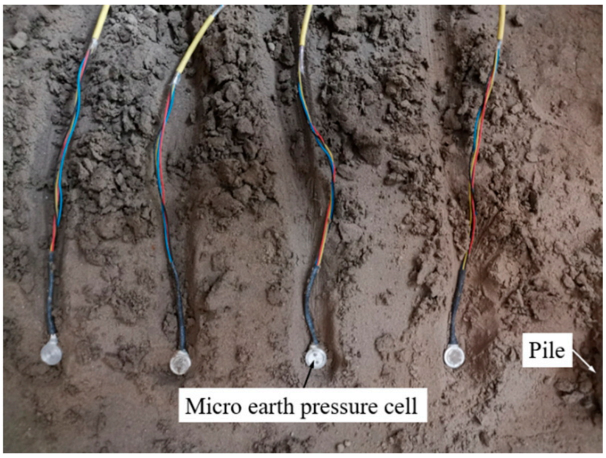

Figure 3. Embedment of micro earth pressure cells.

After completion of the soil filling in the model box, the static load test of the pile can be performed after resting for 20 days. At the end of the model test, ring knives were used to collect soil which is at about 200 mm from the pile axis and 500 mm depth for physical and mechanical tests. The physical and mechanical parameters are shown in Table 2.

Table 2. Physical and mechanical parameters of silt.

Water Content ω (%)	Density P (g/cm^3)	Cohesion c (kPa)	Internal Friction Angle φ (°)	Compression Modulus Es (MPa)	Plasticity Index I_P
9.8	1.61	5	26	8.1	6.4

The static load test of the model pile adopts the slow maintenance load method [24]. The static load test of uplift piles and compressive piles adopts a servo hydraulic loading instrument, which has a displacement sensor and can automatically collect displacement. The compressive pile test diagram is shown in Figure 4.

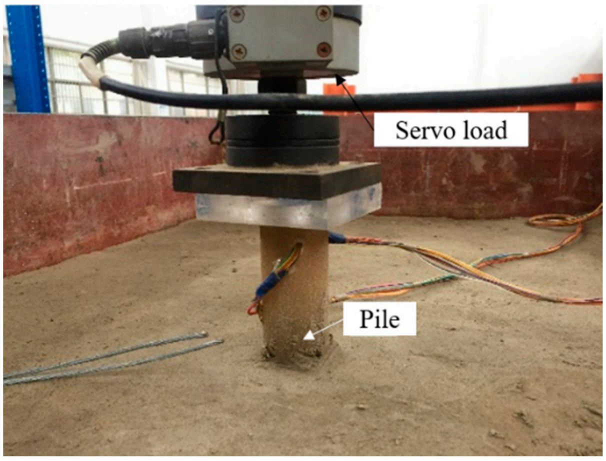

Figure 4. Compressive pile test diagram.

4. Analysis of Test Results

4.1. Load Displacement Relationship of Uplift Pile and Compressive Pile

Figure 5 shows the load-displacement curves (*Q-s* curve) of the uplift pile and compressive pile. We can see from Figure 5, the *Q-s* curves of the uplift pile consist of two sections, which have the characteristics of sudden destroy, the *Q-s* curves of the compressive pile consist of three sections, and have good ductility. Figure 6 shows the displacement-time logarithmic curves (*s-lgt* curve) of the uplift pile and compressive pile. In Figure 5, the *Q-s* curve of the uplift pile rises steeply at a load of 1400 N and the *Q-s* curve of the compressive pile falls steeply at a load of 1700 N. The load at the start of the steep rise or fall is taken as the ultimate bearing capacity [24]. In Figure 6, the *s-lgt* curve of uplift piles does not change linearly when the load is 1500 N, and the *s-lgt* curve of compressive piles does not change linearly when the load is 1800 N, and the first level load before the nonlinear change is taken as the ultimate bearing capacity [24]. From Figures 5 and 6, the ultimate bearing capacities of the uplift pile and compressive pile are determined to be 1400 N and 1700 N, respectively. Both the uplift pile and compressive pile are pure friction piles. The uplift pile produces a negative shaft resistance of 1400 N on the pile side, while the compressive pile produces a positive shaft resistance of 1700 N on the pile side, and the positive shaft resistance is greater than the negative shaft resistance. The uplift coefficient is defined as the shaft resistance of the uplift pile divided by the shaft resistance of the compressive pile, so the uplift coefficient obtained from this test is approximately 0.82.

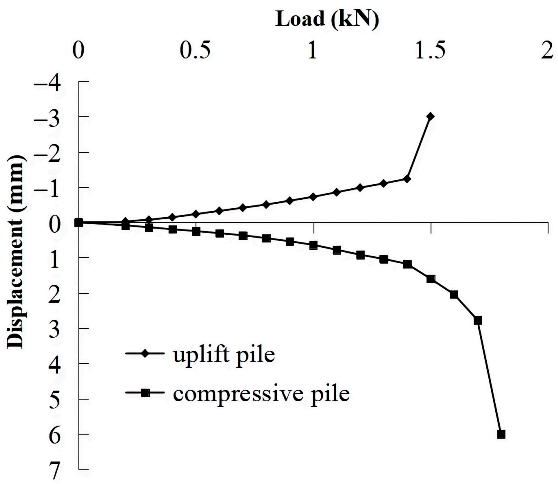

Figure 5. *Q-s* curves of the uplift pile and compressive pile.

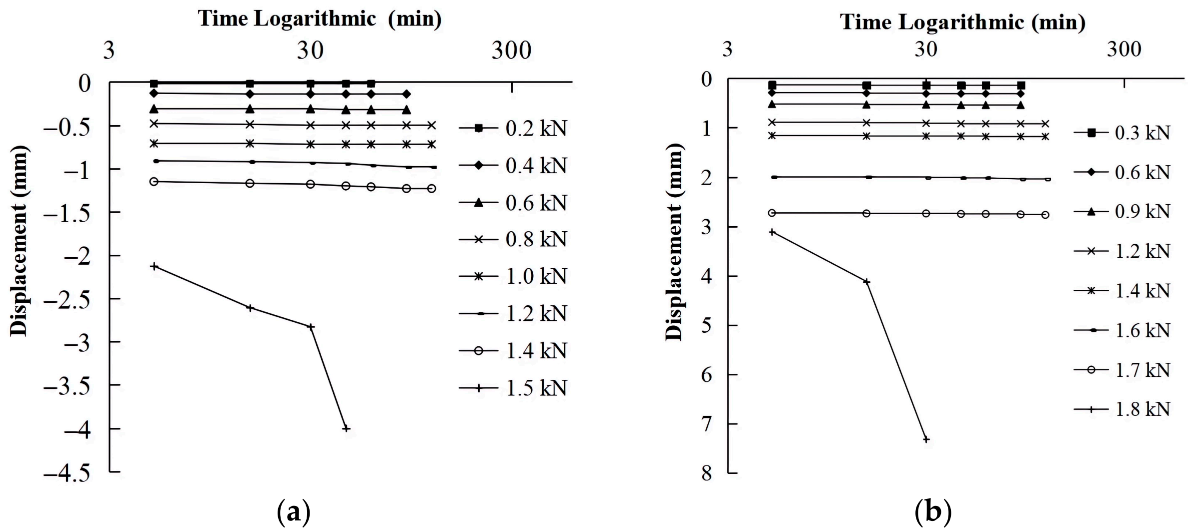

Figure 6. *s-lgt* curves of the uplift pile and compressive pile: (**a**) uplift pile; (**b**) compressive pile.

4.2. Analysis of Additional Stress Caused by Compressive Piles in Soil

4.2.1. Distribution of Additional Stress Caused by Compressive Pile in Soil

When the measured ultimate load is 1700 N, the horizontal distribution of vertical additional stress at different depths around the compressive pile in the soil is shown in Figure 7. From the perspective of depth, the additional stress increases closer to the ground, which is related to the position of the loading point. Closer to the loading point, there is a greater additional stress in the soil, and the loading effect is more obvious. At 75 mm (1.5 d) from the pile axis, the additional stress at 300 mm depth is 0.83 kPa, at 600 mm depth is 0.69 kPa, at 900 mm depth is 0.53 kPa, and at 1200 mm depth is 0.49 kPa.

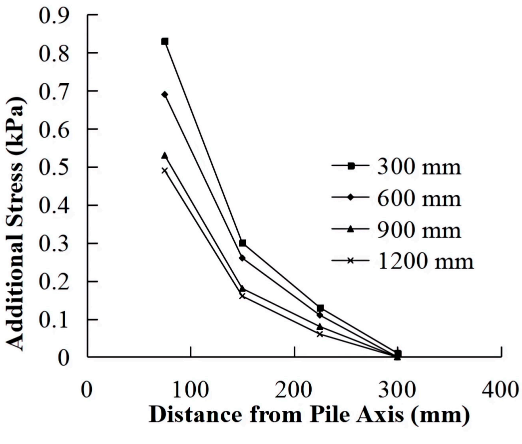

Figure 7. Distribution of additional stress caused by compressive piles in soil.

In the horizontal direction, the additional stress attenuates rapidly along the horizontal direction, showing a steeply decreasing decay up to 150 mm (3 d) from the pile axis and almost zero at 300 mm (6 d) from the pile axis. In the vertical direction, at the depth of 300 mm, 75 mm (1.5 d), 150 mm (3.5 mm (3.0 d), 3.5 d), and 300 mm (6.0 d) from the pile axis, additional stresses are 0.83 kPa, 0.30 kPa, 0.11 kPa, and 0.00 kPa respectively.

4.2.2. Fitting of the Additional Stress Distribution Caused by the Compressive Pile in Soil

The additional stress near the pile surface is used to calculate the shaft resistance of the pile in the soil, but the earth pressure cells buried closest to the pile side in the test are 50 mm away from the pile surface. Therefore, the fitting analysis should be performed according to the existing measured earth pressure distribution curve (the curve is in Figure 7) to determine the additional stress near the pile surface in the soil. After using the exponential fitting, logarithmic fitting, power fitting, and polynomial fitting methods, it was found that the polynomial fit was the best. The polynomial fitting formula of additional stress and fitting results of additional stress near the pile surface is shown in Table 3. From the squared mean square error, the fitting effect of the fitting formula is relatively ideal.

Table 3. Increase in additional stress caused by compressive piles.

Depth (mm)	Fitting Formula	Squared Mean Square Error	σ_{z0} (kPa)
300	$\sigma_z = 0.00002x^2 - 0.0103x + 1.4875$	0.9878	1.2425
600	$\sigma_z = 0.00001x^2 - 0.0083x + 1.22$	0.9895	1.01875
900	$\sigma_z = 0.00001x^2 - 0.0083x + 1.22$	0.9838	0.79375
1200	$\sigma_z = 0.00001x^2 - 0.0066x + 0.9075$	0.9847	0.74875

Notation: σ_z is the vertical additional stress; x is the distance from the calculation point to the pile axis; σ_{z0} is the vertical additional stress near the pile surface.

4.3. Analysis of Additional Stress Caused by Uplift Piles in Soil

4.3.1. Distribution of Additional Stress Caused by Uplift Piles in Soil

The horizontal distribution of vertical additional stress at different depths around the uplift pile in the soil is shown in Figure 8 when the measured ultimate load is 1400 N. The loading direction is upward, and the pile moves upward relative to the soil, so the direction of additional stress generated in the soil is also upward. It shows the unloading effect for the soil, which is expressed as a negative value. The closer to the loading point, the greater the unloading effect caused by the additional stress in the soil in Figure 8. At 75 mm (1.5 d) from the pile axis, the additional stresses at the depth of 300 mm, 600 mm, 900 mm, and 1200 mm are −0.72 kPa, −0.65 kPa, −0.58 kPa and −0.55 kPa respectively. In the horizontal direction, the distribution of the additional stress is similar to that of the compressive pile, and the additional stress rapidly attenuates. It shows a steep decline within 150 mm (3 d) from the pile axis. The additional stress is almost zero at 300 mm (6 d) from the pile axis. At the depth of 300 mm, 75 mm (1.5 d), 150 mm (3.0 d), 225 mm (4.5 d), and 300 mm (6.0 d) from the pile axis, the additional stresses are −0.72 kPa, −0.25 kPa, −0.07 kPa and 0.00 kPa, respectively.

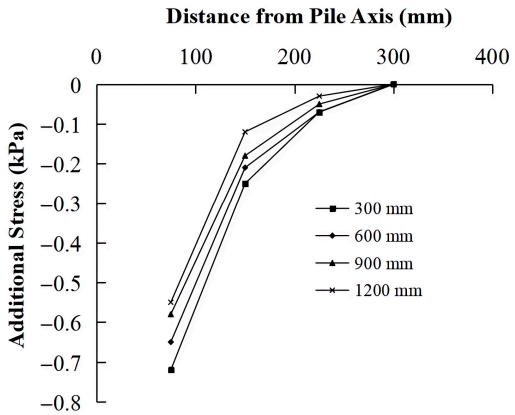

Figure 8. Distribution of additional stress caused by uplift piles in soil.

4.3.2. Fitting of Additional Stress Distribution Caused by Uplift Piles in Soil

The four curves of the horizontal distribution of the additional stress at different depths were fitted to obtain the fitting formula of the four curves in Figure 8. The fitting formula of additional stress and fitting value of additional stress near the pile surface is shown in Table 4. Because the uplift pile load is upward, the direction of additional stress is also upward in the soil, which is expressed by a negative value.

Table 4. Decrease in additional stress caused by the uplift pile.

Depth (mm)	Fitting Formula	Squared Mean Square Error	σ_{z0} (kPa)
300	$\sigma_z = -0.00002x^2 + 0.0098x - 1.345$	0.9949	−1.1125
600	$\sigma_z = -0.00002x^2 + 0.009x - 1.2175$	0.9896	−1.005
900	$\sigma_z = -0.00002x^2 + 0.0083x - 1.1075$	0.9913	−0.9125
1200	$\sigma_z = -0.00002x^2 + 0.009x - 1.11$	0.9799	−0.8975

Notation: σ_z is the vertical additional stress; x is the distance from the calculation point to the pile axis; σ_{z0} is the vertical additional stress near the pile surface.

4.4. Calculation and Analysis of the Shaft Resistance of the Pile

A compressive pile with no soil at the bottom is a pure friction pile, and its bearing capacity is the sum of the shaft resistance on the pile surface area, i.e., its bearing capacity represents the shaft resistance of the pile.

According to Fleming et al. [25], the initial shaft resistance of pile τ_s can be expressed as:

$$\tau_{s0} = \sigma_n^{'} \tan\delta = K\sigma_v^{'} \tan\delta \tag{1}$$

where the $\sigma_n^{'}$ is the normal effective stress on the pile surface; the δ is the friction angle between the pile surface and soil. According to Kulhawy et al. [26], δ/φ of smooth concrete piles is 0.8~1.0, δ/φ of rough pile surfaces is 1.2, and φ is the internal friction angle of the soil. The K is the coefficient of vertical effective stress converted to the horizontal effective stress, which is 1.2 [25]; the $\sigma_v^{'}$ is the vertical effective stress of soil.

When there is vertical additional stress σ_z in soil, Equation (1) can be rewritten as:

$$\tau_{s1} = \sigma_n^{'} \tan\delta = K\left(\sigma_v^{'} + \sigma_z\right) \tan\delta \tag{2}$$

We can calculate the shaft resistance of the pile by Equation (2) when considering the additional stress in the soil.

According to Equations (1) and (2), the calculated initial shaft resistance of pile τ_{s0} and shaft resistance τ_{s1d} after accounting for the influence of additional stress in the soil are shown in Table 5. $(\tau_{s1d} - \tau_{s0})/\tau_{s0}$ represents an increased value of the shaft resistance of pile. The shaft resistance of pile τ_{s1d} increases after considering the additional stress in Table 5. A shorter distance to the loading point corresponds to a greater increase in the shaft resistance of the pile. This result indicates that the loading effect of pile side soil caused by compressive piles is more obvious. At the depth of 300 mm, 600 mm, 900 mm, and 1200 mm, the improvement rate of the shaft resistance is 25.4%, 10.4%, 5.4%, and 3.8%, respectively.

Table 5. Increase in shaft resistance of the compressive pile.

Depth (mm)	τ_{s0} (kPa)	τ_{s1d} (kPa)	$((\tau_{s1d}-\tau_{s0})/\tau_{s0})$ (%)
300	3.37	4.23	25.4
600	6.74	7.45	10.4
900	10.12	10.66	5.4
1200	13.49	14.01	3.8
Average value	8.43	9.09	11.3

The initial shaft resistance of pile τ_{s0} calculated by Equation (1) and the shaft resistance of the pile τ_{s1u} after accounting for the influence of additional stress calculated by Equation (2), are shown in Table 6. Considering the additional stress after the unloading effect, the calculated shaft resistance of the pile τ_{s1u} is less than the initial shaft resistance of the pile τ_{s0}. A shorter distance to the loading point corresponds to a more obvious decrease in shaft resistance of the pile and a more obvious unloading effect of the pile side soil due to the uplift pile. The vertical stress decrease rate is 22.8% at 300 mm from the loading point, 10.3% at 600 mm, 6.2% at 900 mm, and 4.3% at 1200 mm, and the average shaft resistance decrease rate of the entire pile is approximately 11%.

Table 6. Decrease in shaft resistance of the uplift pile.

Depth (mm)	τ_{s0} (kPa)	τ_{s1d} (kPa)	$((\tau_{s1d} - \tau_{s0})/\tau_{s0})$ (%)
300	3.37	2.61	−22.8
600	6.74	6.05	−10.3
900	10.12	9.49	−6.2
1200	13.49	12.87	−4.6
Average value	8.43	7.75	−11.0

4.5. Analysis of the Difference in Shaft Resistance between Uplift Piles and Compressive Piles

The shaft resistance of the uplift pile τ_{s1u} and shaft resistance of the compressive pile τ_{s1d} are listed in Table 7. Table 7 shows that a shorter distance to the loading point corresponds to a greater difference in shaft resistance between the uplift pile and compressive pile. This result indicates that the unloading effect caused by uplift piles and the loading effect caused by compressive piles are greater. Considering the loading and unloading effects, the calculated uplift coefficient is λ = 0.85. Compared with the measured uplift coefficient of λ = 0.82, the calculated uplift coefficient of 0.85 is very close to the measured uplift coefficient. This result indicates that the loading and unloading effects of soil are the main reason for the lower shaft resistance of uplift piles compared to compressive piles.

Table 7. Comparison of the shaft resistance of uplift piles and compressive piles.

Depth (mm)	τ_{s0} (kPa)	τ_{s1d} (kPa)	$-\tau_{s1u}/\tau_{s1d}$
300	2.61	4.23	0.62
600	6.05	7.45	0.81
900	9.49	10.66	0.89
1200	12.87	14.01	0.92
Average value	7.75	9.09	0.85

4.6. Calculated and Measured Values of Uplift Bearing Capacity

Meyerhof [9], Deshmukh [11] and other researchers have proposed formulas to calculate the ultimate bearing capacity of uplift piles. To make comparisons, the values calculated by Meyerhof's formula (1973), Deshmukh's formula (2010), and this paper's method (which considers the loading and unloading effects) and the test values are listed in Table 8. The uplift bearing capacity calculated after considering the unloading effect of uplift piles is very close to the bearing capacity calculated by Meyerhof's formula (1973), Deshmukh's formula (2010), and the test bearing capacity. Therefore, the method proposed here to calculate the shaft resistance of uplift piles considering the unloading effect is practical.

Table 8. Calculated and measured values of the ultimate bearing capacity of the uplift pile.

Meyerhof (1973)	Deshmukh (2010)	Method of This Paper	Measured Value
1472	1451	1441	1400

Notation: Unit N in the table.

5. Conclusions

Static load tests were carried out on the uplift and compressive piles respectively. The vertical additional stresses caused by the uplift and compressive piles in the surrounding soil were measured by burying micro earth pressure cells in the soil. After polynomial fitting, the vertical additional stresses immediately adjacent to the pile side were obtained, and a method for calculating the shaft resistance considering the loading and unloading effects was proposed, the following conclusions are obtained after analysis:

1. The maximum influence range of the additional stress in the soil caused by pile loading is approximately 6 d from the axis of the pile;
2. The uplift pile shows an unloading effect on the surrounding soil, while the compressive pile shows a loading effect on the surrounding soil. A shorter distance to the loading point corresponds to a more obvious unloading effect of the uplift pile and loading effect of the compressive pile;
3. The uplift bearing capacity of the pile is less than the compressive bearing capacity due to the difference between the unloading effect of the uplift pile and the loading effect of the compressive pile, the shaft resistance of the uplift pile is about 0.85 times that of the compression pile;
4. The uplift capacity calculated using the loading and unloading effects proposed in this paper is close to the measured uplift bearing capacity, the method can be applied to calculate the bearing capacity of uplift piles.

Author Contributions: Conceptualization, H.M.; methodology, H.M.; software, Y.M.; validation, H.M.; formal analysis, H.M.; investigation, H.M.; resources, H.M.; data curation, H.M.; writing—original draft preparation, H.M.; writing—review and editing, H.M. and H.Z.; visualization, L.Z. and H.Z.; supervision, H.M.; project administration, H.M.; funding acquisition, H.M. All authors have read and agreed to the published version of the manuscript.

Funding: This research was funded by the National Natural Science Foundation of China, grant number 51878618.

Institutional Review Board Statement: Not applicable.

Informed Consent Statement: Not applicable.

Data Availability Statement: Data are contained within the article.

Conflicts of Interest: The authors declare no conflict of interest. The funders had no role in the design of the study; in the collection, analyses, or interpretation of data; in the writing of the manuscript, or in the decision to publish the results.

References

1. Li, F.; Song, Q. Study on discrete element particle flow of multi-layered ground-based expanded bottom uplift pile. *J. Cent. South. Univ. (Sci. Technol.)* **2019**, *50*, 2856–2859.
2. Huang, S.; Zhou, J.J.; Gong, X.N. Experimental study on bearing capacity of pre-bored grouted planted pile under compression and tension. *J. Hunan. Univ. (Nat. Sci.)* **2021**, *48*, 30–36.
3. Cao, W.P.; Tao, P.; Li, S. Model experiment on bearing deformation behavior of uplift pedestal piles. *Xi'an Univ. Arch. Tech.* **2020**, *52*, 30–37.
4. Lai, Y.; Jin, G.F. Uplift behavior and load transfer mechanism of prestressed high-strength concrete piles. *J. Cent. South. Univ. Technol.* **2010**, *17*, 136–141. [CrossRef]
5. Basha, A.; Azzam, W.R. Uplift capacity of single pile embedded in partially submerged sand. *KSCE J. Civil. Eng.* **2018**, *22*, 4882–4890. [CrossRef]
6. Emirler, B.; Tolun, M.; Yildiz, A. An experimental study of rough single pile and pile group under uplift loading in sand. *Eur. J. Environ. Civ. Eng.* **2019**, *25*, 557–574. [CrossRef]
7. Ashour, M.; Abbas, A. Response of piles in multilayers of soil under uplift forces. *Int. J. Geom.* **2020**, *20*, 04020056. [CrossRef]
8. Das, B.M. A procedure for estimation of uplift capacity of rough piles. *Soils Found.* **1983**, *23*, 122–126. [CrossRef]
9. Meyerhof, G.G. Uplift resistance of inclined anchor and piles. In Proceedings of the 8th International Conference on Soil Mechanics and Foundation Engineering, Moscow, Russia, August 1973; Volume 12, pp. 167–173.
10. Chattopadhyay, B.C.; Pise, P.J. Uplift capacity of piles in sand. *J. Geotech. Eng. Div. ASCE* **1986**, *112*, 888–904. [CrossRef]
11. Deshmukh, V.B.; Dewaikar, D.M.; Choudhury, D. Computations of uplift capacity of pile anchors in cohessionless soil. *Acta Geotech.* **2010**, *5*, 87–94. [CrossRef]
12. Tovar-Valencia, R.D.; Galvis-Castro, A.; Salgado, R.; Prezzi, M. Effect of surface roughness on the shaft resistance of displacement model piles in sand. *J. Geotech. Geoenvironmental.* **2018**, *144*, 1943–5606. [CrossRef]
13. Galvis-Castro, A.C.; Tovar-Valencia, R.D.; Salgado, R.; Prezzi, M. Effect of loading direction on the shaft resistance of jacked piles in dense sand. *Geotechnique* **2019**, *69*, 16–28. [CrossRef]
14. Denicola, A.; Mark, F.R. Tensile and compressive shaft capacity of piles in sand. *J. Geotech. Eng.* **1993**, *119*, 1952–1973. [CrossRef]
15. Wang, Y.Q.; Zhang, L. Research on bearing capacity behavior of up lift pile. *J. Harbin Inst. Technol.* **2006**, *38*, 389–391.

16. Zhang, Z.M.; Liu, N.W.; Fang, K. Influence of Poisson's effect on uplift coefficient considering tip resistance. *Chin. J. Geotech. Eng.* **2011**, *33* (Suppl. S2), 494–497.
17. Su, D.; Zhao, P.; Gao, X. An elastic-plastic load-transfer model considering Poisson's effect. *Rock Soil Mech.* **2015**, *36*, 2799–2803.
18. Ou, M.X.; Dai, Z.F.; Chen, Y.H. Load transfer model considering over-consolidation ratio and Poisson effect. *J. Chongqing Univ.* **2020**, *43*, 101–108.
19. Wang, X.J.; Wu, J.B.; Huang, M.S. Influence of the Poisson's effect on the anti-uplift coefficient of uplift pile. *Chin. J. Undergr. Spa. Eng.* **2009**, *5* (Suppl. S2), 1545–1548.
20. Ma, H.L.; Bao, Y.R.; Ma, Y.F.; Yao, W.H.; Yang, B.L. Research on model tests of the additional stress in soil caused by pile loads. *Soil Mech. Found. Eng.* **2021**, *58*, 332–338. [CrossRef]
21. Ma, H.L.; Ma, Y.F.; Zhang, H.Y. Experimental research on the additional stress characteristics in soil caused by a self-anchored test pile. *Arabian J. Geosci.* **2022**, *15*, 396. [CrossRef]
22. Zhou, Y.; Ling, Y.Q.; Yang, X.H. Relationship between the displacement and stability of pile anchor retaining structure considering additional stress. *Rock Soil Mech.* **2018**, *39*, 2913–2921.
23. Mindlin, R.D. Force at a point in the interior of a semi-infinite solid. *Physics* **1936**, *7*, 195–202. [CrossRef]
24. *JGJ 106-2014*; Technical Code for Testing of Building Foundation Piles. China Architecture & Building Press: Beijing, China, 2014.
25. Fleming, K.; Weltman, A.; Randolph, M. *Piling Engineering*; Taylor & Francis: Abingdon, UK, 2009.
26. Kulhawy, F.H. Limiting tip and side resistance. In Proceedings of the Symposium on Analysis and Design of Pile Foundation, San Francisco, CA, USA, 1–5 October 1984; pp. 80–98.